

# 1 **Energy states of soil water – a thermodynamic perspective on soil** 2 **water dynamics and storage controlled stream flow generation in** 3 **different landscapes**

4 Erwin Zehe<sup>1</sup>, Ralf Loritz<sup>1</sup>, Conrad Jackisch<sup>1</sup>, Martijn Westhoff<sup>2</sup>, Axel Kleidon<sup>3</sup>, Theresa Blume<sup>4</sup>,  
5 Sibylle, K. Hassler<sup>1</sup>, Hubert, H. Savenije<sup>5</sup>

6 1) Karlsruhe Institute of Technology (KIT), 2) Vrije Universiteit Amsterdam, The Netherlands, 3),  
7 Max Planck Institute for Bio-Geo-Chemistry, Jena 4), GFZ German Research Centre for Geosciences  
8 5) Delft Technical University.

9 Abstract: The present study corroborates that a thermodynamic perspective on soil water is  
10 well suited to distinguish the typical interplay of gravity and capillarity controls on soil water  
11 dynamics in different landscapes. To this end, we express the driving matrix and gravity  
12 potentials by their energetic counterparts and characterize soil water by its free energy state.  
13 The latter is the key to defining a new system characteristic determining the possible range of  
14 energy states of soil water, reflecting the joint influences of soil physical properties and height  
15 over nearest drainage (HAND) in a stratified manner. As this characteristic defines the  
16 possible range of energy states of soil water in the root zone, it also allows an instructive  
17 comparison of top soil water dynamics observed in two distinctly different landscapes. This is  
18 because the local thermodynamic equilibrium at a given HAND and the related equilibrium  
19 storage allow a subdivision of the possible free energy states into two different regimes.  
20 Wetting of the soil in local equilibrium implies that free energy of soil water gets positive,  
21 which in turn implies that the soil is in a state of a storage excess. While further drying of the  
22 soil leads to a negative free energy and a state of a storage deficit. We show that during one  
23 hydrological year the energy states of soil water visit distinctly different parts of their  
24 respective energy state spaces. Both study areas exhibit furthermore a threshold-like relation  
25 between the observed free energy of soil water in the riparian zone and observed streamflow,  
26 while the tipping points coincide with the local equilibrium state of zero free energy. We  
27 found that the emergence of a potential energy excess/storage excess in the riparian zone  
28 coincides with the onset of storage controlled direct streamflow generation. While such  
29 threshold behavior is not unusual, it is remarkable that the tipping is consistent with the  
30 underlying theoretical basis.

# 31 1 INTRODUCTION

## 32 1.1 Motivation

33 Only a minute amount of global water is stored in the root zone of the soil. Yet this tiny  
34 storage compartment crucially controls a variety of processes and ecosystem functions. The  
35 root soil water stock essentially supplies savannah vegetation (e.g. Tietjen et al., 2009; Tietjen  
36 et al. 2010) and more generally ecosystems during severe droughts (Gao et al., 2014). The soil  
37 water content controls infiltration, runoff formation and streamflow generation (Graeff et al.,  
38 2009; Zehe et al., 2010), it partly determines habitat quality of earthworms (e.g. Schneider et  
39 al.; 2018) and it is of key importance for soil respiration and emission of greenhouse gases in  
40 mountain rain forests (e.g. Koehler et al., 2012). Soil water dynamics is thereby controlled by  
41 the triple of infiltration, moisture retention and water release. These processes are driven by  
42 the intermittent rainfall and radiative forcing and controlled by multiple forces arising from  
43 capillarity, gravity, root water uptake and optionally osmosis. Steady state, hydraulic  
44 equilibrium conditions imply that the driving forces act in a balanced manner. In the simple  
45 case of absent vegetation and of a flat topography this force balance corresponds to the well-  
46 known hydraulic equilibrium, where the matric potential equals the negative of the gravity  
47 potential along the entire soil profile. The corresponding equilibrium soil water content  
48 profile, which is straightforward to calculate if depth to groundwater and the soil water  
49 retention curve are known, reflects thus a balance between the most the prominent influences:  
50 the local capillary control and the non-local gravitational control. Although these two controls  
51 are sensitive to distinctly different systems properties, these properties are not necessarily  
52 independent. The climatological and geological setting constraints the co-development or co-  
53 evolution of soils, geomorphology and vegetation (as suggested by e.g. Troch et al., 2015;  
54 Sivapalan and Blöschl, 2015; Saco and Moreno-de las Heras, 2013). One might hence wonder  
55 whether this constraint co-development created a distinctly typical interplay of capillary and  
56 gravitational controls on soil moisture. In the present study we show that this interplay  
57 manifests through a) distinct differences in soil water dynamics among different hydrological  
58 landscapes and b) a thermodynamic perspective on soil water dynamics to discriminate  
59 typical differences that cannot be inferred from the usual comparison of soil moisture  
60 observations.

## 61        **1.2 Thermodynamic reasoning in hydrology and related earth sciences**

62 Thermodynamic reasoning has a long tradition in earth science, ecology and hydrology and  
63 one of its key advantages is a joint treatment of mass fluxes and the related conversions of  
64 energy, including dissipation and entropy production. In geomorphology its dates back to the  
65 early work of Leopold and Langbein (1962) on the role of entropy in the evolution of  
66 landforms. Howard (1971, cited in Howard 1990) proposed that angles of river junctions are  
67 arranged in such way that they minimize stream power. Bolt and Frissel (1960) related soil  
68 water potentials to Gibbs free energy of soil water (referring to the early pioneers Edelfson  
69 and Anderson (1940)) and established a link between soil physics and thermodynamics. In  
70 ecology Lotka (1922a; 1992b) proposed that organisms that maximize their energy through  
71 put, have an advantage within the evolutionary selection process.

72 Thermodynamics gained substantial attention in catchment hydrology since the work of  
73 Reggiani et al. (1998a) and of Kleidon and Schymanski (2008). Reggiani et al. (1998a)  
74 employed thermodynamic reasoning and volume averaging to derive a model framework of  
75 intermediate complexity (Sivapalan, 2018). They introduced the idea of a representative  
76 elementary watershed REW, which can be seen as least spatial entity for building mesoscale  
77 hydrological models. This idea has been picked up and advanced by several follow-up studies  
78 dealing with the coding and successful application of REW-based hydrological models  
79 (Reggiani et al., 1998a; Reggiani et al., 1998b; Reggiani et al., 1999; Reggiani et al., 2000;  
80 Reggiani and Schellekens, 2003; Lee et al., 2005; Zhang et al., 2006; Tian et al., 2006; Lee et  
81 al., 2007) or the challenge to derive the necessary closure relations (Zehe et al., 2006; Beven,  
82 2006).

83 Along a different avenue, Kleidon and Schymanski (2008) discussed the opportunity of using  
84 maximum entropy production (MEP, originally proposed by Paltridge, 1979) to predict steady  
85 state, close to equilibrium functioning of hydrological systems and to infer model parameters  
86 based on thermodynamic optimality. This idea has motivated several efforts to predict the  
87 catchment water balance using thermodynamic optimality. For instance, Porada et al. (2011)  
88 simulated the water balance of the 35 largest basins on Earth using the SIMBA model and  
89 inferred parameters controlling root water uptake by maximizing entropy production. They  
90 tested the plausibility of their assessment within the Budyko framework (Budyko 1958). Zehe  
91 et al. (2013) showed that a thermodynamic optimum density of macropores created by worm  
92 burrows which maximized dissipation of free energy during recharge events allowed an  
93 acceptable uncalibrated prediction of the rainfall runoff response of a lower mesoscale

94 catchment with a physically based hydrological model. While this finding is at least an  
95 interesting incidence, the explanation why the worms should create their burrows in such a  
96 way is not straightforward. Hildebrandt et al. (2017) proposed that plants optimize their root  
97 water uptake by minimizing the necessary energetic investment through a spatially uniform  
98 water abstraction from uniform soils. Along similar lines of thought but at much larger scales  
99 Gao et al., (2014) proposed that ecosystems optimize their rooting depth. This is deemed to  
100 balance the advantage of vegetation to endure droughts of increasing return periods with the  
101 necessary energetic investment to expand their root system to enlarge the water holding  
102 capacity.

103 Kleidon et al. (2013) tested whether the topology of connected river networks can be  
104 explained through a maximization of kinetic energy transfer to sediment flows. They showed  
105 that the depletion of topographic gradients by sediment transport can be linked to a  
106 minimization in frictional dissipation in streamflow networks, which in turn implies a  
107 maximization of sediment flows against the topographic gradient and thus of power in the  
108 sediment flows. The idea that the topology of river networks reflects an energetic  
109 optimum - more precisely a minimum - is in fact much older and was already suggested by  
110 Howard (1990) and picked up by Rinaldo et al. (1996) as concept of minimum energy  
111 expenditure. Hergarten et al. (2014) transferred this idea to groundwater systems by analyzing  
112 preferential flow paths that minimize the total energy dissipation at a given recharge under the  
113 constraint of a given total porosity and by verifying those against data sets for spring  
114 discharge in the Austrian Alps.

115 Kleidon et al. (2014) and Renner et al. (2016) tested whether a two-layer energy balance  
116 model based on maximum power in combination with Carnot efficiency is suited to predict  
117 the partitioning of net short wave radiation into long wave outgoing radiation and turbulent  
118 fluxes of latent and sensible heat. During convective conditions their predictions were in good  
119 accordance with flux tower data at three sites with different land use.

120 While some of us might find the search for thermodynamic optimality exciting and promising,  
121 it is certainly not the Philosophers stone. Westhoff et al. (2013) found for instance that a  
122 conceptual model structure which was in accordance with MEP was not suited to predict  
123 timing of the water balance in the HJ Andrews experimental watershed. Thermodynamic  
124 optimality should thus be seen as a testable and sometimes helpful constraint, but it should not  
125 be mixed with a first principle such as the first and second law of thermodynamics (Westhoff  
126 et al. 2019). And thermodynamic optimality is restricted to explain system steady state, close

127 to equilibrium functioning. The challenge is however to explain operation of hydrological  
128 systems under temporarily variable forcing (Westhoff et al. 2014) and far from equilibrium  
129 conditions.

130 In summary we think that there are four general arguments why a thermodynamic perspective  
131 on soil water dynamics and hydrology in general has much to offer. Firstly, surface runoff and  
132 particularly soil water fluxes dissipate a very large amount of their driving energy differences.  
133 As the dissipation and related entropy production rates depend on the soil material and on the  
134 spatial organization of the material as well (Zehe et al., 2010), one may quantify feedbacks  
135 between morphological/structural changes and hydrological processes within the same  
136 current. Secondly, energy is an extensive quantity, as such it is additive when different  
137 systems are merged, it grows with increasing system size and changes can be described  
138 through a balance. One may hence apply volumetric averaging and upscaling to energy for  
139 instance to derive macroscale effective constitutive relations and macroscale equations as  
140 shown by de Rooij (2009, 2011). In contrary the related gravity and matric potentials are  
141 intensive state variables and as such neither additive in the above specified sense, nor can  
142 their changes be balanced. Thirdly, it can be used to define and explain hydrological  
143 similarity based on a thermodynamically meaningful combination of catchment characteristics  
144 (Zehe et al., 2014; Seibert et al., 2017; Loritz et al., 2018). Last but not least, one may test  
145 whether thermodynamic optimality provides, despite of the fact that it is controversial, a  
146 means to test the recent proposition of Savenije and Hrachowitz (2017), stating that:  
147 ‘Ecosystems control the hydrological functioning of the root zone in a way that it  
148 *continuously* optimizes the functions of infiltration, moisture retention and drainage of  
149 catchments.’

### 150 **1.3 Objectives**

151 In the following, we show that the free energy state of soil water is well suited for  
152 characterizing distinct differences in soil water dynamics among different landscapes. Based  
153 on the free energy state we define a system characteristic, which jointly accounts for the  
154 capillary and gravitational control of soil water dynamics, using height over the nearest  
155 drainage (HAND, Renno et al., 2008; Nobre et al., 2011) as a proxy for the gravity potential.  
156 These energy state functions are strongly sensitive to differences in topography and soil water  
157 characteristics of our two study areas and allow an instructive visualization of soil water  
158 dynamics in energetic terms. This reveals that the soil water stock in both landscapes operates  
159 distinctly differently with respect to the local thermodynamic equilibrium state of minimum

160 free energy. More specifically we provide evidence that the local thermodynamic equilibrium  
161 state separates two regimes of a storage deficit and storage excess. During a one year period  
162 the observed energy states of the soil water in the study areas operated distinctly differently  
163 with respect to these regimes and visited distinctly different ranges of their corresponding  
164 energetic state space. Last but not least we provide evidence that the state of zero free energy  
165 does not only separate regimes of a storage deficit and a storage excess, it is furthermore also  
166 a theoretically motivated threshold, explaining the onset of storage controlled direct runoff  
167 production in our study areas.

## 168 **2 THEORETICAL BACKGROUND**

169 In the following we express the matric and gravity potentials by their energetic counterparts,  
170 following largely the work of Bolt and Frissel (1960) and de Rooij (2009), to characterize soil  
171 water storage by its free energy state and derive the energy state function.

### 172 **2.1 Free energy of the soil water**

173 Following the micro approach of Bolt and Frissel (1960) we start our derivation with the  
174 Gibbs free energy  $G$  (J) of a small soil volume  $V$  that contains a test body of water with mass  
175  $M$  (kg). Assuming isotherm conditions, while neglecting osmotic forces and the energy of  
176 water adsorption leads to:

$$177$$
$$178 \quad dG_{\text{free}} = VdP_e + V_w dp + Mgdz \quad \text{Eq. (1)}$$
$$179$$

180 Where  $g$  ( $\text{ms}^{-2}$ ) is gravitational acceleration,  $dz$  (m) denotes a change in position in the gravity  
181 field,  $P_e$  ( $\text{Nm}^{-2}$ ) is the external pressure,  $p$  ( $\text{Nm}^{-2}$ ) is the capillary pressure,  $dp$  the local  
182 pressure increment, which relates to the capillary pressure difference between water and air,  
183  $V_w$  is the volume of the test water body. Please note that Eq. 1 is not total differential, this is  
184 why classical text books of thermodynamics use the symbol  $\delta$  instead of the  $d$ , and speak of a  
185 variation in pressure or elevation.

186 In the next step, we express Eq. 1 as a change in volumetric energy density. When recalling a)  
187 that  $V_w$  equals the product of  $V$  and the soil water content  $\theta$  ( $\text{m}^3\text{m}^{-3}$ ) and b) that the water  
188 mass  $M$  equals the product of its density  $\rho$  ( $\text{kgm}^{-3}$ ),  $V$  and  $\theta$ , we obtain:

189

190 
$$dg_{\text{free}} = \overbrace{dP_e}^{\text{Work}} + \overbrace{\theta dp}^{\text{capillaryenergy}} + \overbrace{\rho g \theta dz}^{\text{potentialenergy}} \quad \text{Eq. (2)}$$

191  
 192 The first term on the right-hand side is mechanical work per volume due to external pressure  
 193 changes (for instance compression), the second term relates to changes in Gibbs free energy  
 194 density related to capillary pressure changes, while the last term related to changes in  
 195 potential energy of the gravity field. In the following the work term is neglected, as we are  
 196 interested in those changes in Gibbs free which relate to dynamic changes in the stored water  
 197 amount. As capillary pressure is equal to the product of matric potential  $\psi$  (m) times the unit  
 198 weight of water Eq. (2) can be reformulated as follows:

199  
 200 
$$dg_{\text{free}} = \rho g \theta d\psi + \rho g \theta dz \quad \text{Eq. (3)}$$

201  
 202 While we acknowledge that the first term on the right hand side is often referred to as matric  
 203 potential energy (see e.g. Hillel, 2001), we think that the adjective potential is misleading due  
 204 the correct meaning of potential energy and shortly explain why we deviate from established  
 205 terminology here. Potential energy refers to the position of a test body of mass M in the  
 206 gravity field and remains invariant when the inner state of the test (soil) body changes, for  
 207 instance through compression, when exchanging the fluid mass in the pore space by the same  
 208 mass of a different fluid. The Young-Laplace equation tells us that both operations change the  
 209 matric potential in soil, either through a compaction of the soil pores and a reduced pore  
 210 radius  $r$  (m) or through the change in surface tension  $\sigma$  (N/m):

211  
 212 
$$\psi = -\frac{2\sigma \cos \phi}{\rho g} \left( \frac{1}{r_{\text{max}}} - \frac{1}{r_{\text{min}}} \right) \quad \text{Eq. (4)}$$

213  
 214 Where  $\phi$  is the wetting angle. As this form of energy depends on the inner structure of the soil  
 215 and on the chemical properties of the fluid, does partly determine the inner energy of the soil  
 216 body in a thermodynamic sense, more precisely it relates to surface energy. We thus refer to  
 217 term 1 in Eq. 3 as ‘capillary binding energy’, consistently with Zehe et al. (2013).

218  
 219 When deriving Eq. (3) with respect to time (and neglecting changes in  $z$ ) we find that a  
 220 change in soil water content implies a change in its free energy state:

221

222 
$$\frac{\partial g_{\text{free}}}{\partial t} = \frac{\partial (e_{\text{pot}} + e_{\text{cap}})}{\partial t} = \rho g \left[ (\psi + z) \frac{d\psi}{d\theta} \frac{\partial \theta}{\partial t} + z \frac{\partial \theta}{\partial t} \right] \text{ Eq. (5).}$$

223

224 Note that the potential energy density of soil water (the second term on the right hand side)  
225 grows linearly with increasing soil water content. On the contrary capillary binding energy  
226 shrinks with growing soil water content, as the absolute value of the matric potential declines  
227 non-linearly with increasing soil water content. The change in capillary energy density with a  
228 given change in soil water content is determined by the product of the actual soil water and  
229 the slope of the water retention curve. We thus state that the product of the well-known soil  
230 hydraulic potential,  $\psi + z$ , and the soil water content corresponds to the volumetric density of  
231 free energy of soil water per unit weight. The free energy of soil water for a larger volume is  
232 the volume integral of the total hydraulic potential times the soil water content over the  
233 volume of interest (de Rooij, 2009; Zehe et al., 2013):

234

235 
$$E_{\text{free}} = E_{\text{cap}} + E_{\text{pot}} = \int \rho g (\psi(\theta) + z) \theta dV \text{ Eq. (6)}$$

236

237 The latter reflects both the binding state and the amount of water that is stored in a control  
238 volume at a given elevation above groundwater and thus reflects the local retention properties  
239 and the topographic setting as well. Not the change in potential energy of soil water at a given  
240 elevation scales linearly with the soil water content. One might thus wonder whether the  
241 dominance of the one or the other energy form may at least partly influence whether a system  
242 behaves in a linear or non-linear fashion.

243

## 244 **2.2 Hydraulic equilibrium, thermodynamic equilibrium and related soil** 245 **water content**

246 The state of minimum Gibbs free energy corresponds to a state of maximum entropy and thus  
247 to thermodynamic equilibrium. With respect to Eq. (3) this is the case when gravity and  
248 matric potential are equal in absolute terms in the entire profile of the unsaturated zone:

249

250 
$$\begin{aligned} d\psi &= -dz \Leftrightarrow \\ \psi &= -z + c \end{aligned} \text{ (Eq. 7).}$$



251

252 The integration constant  $c$  in Eq. (7) is, as it is well known, equal to zero as the matric  
253 potential is zero at the groundwater surface, for  $z=0$ . In hydraulic equilibrium the absolute  
254 value of Gibbs free energy of soil water is thus equal to zero. And the related soil water  
255 content, which balances capillary and gravitational influences, is straightforwardly calculated  
256 by substituting the matric potential in the soil water retention curve with the depth above  
257 groundwater, when the latter is known.

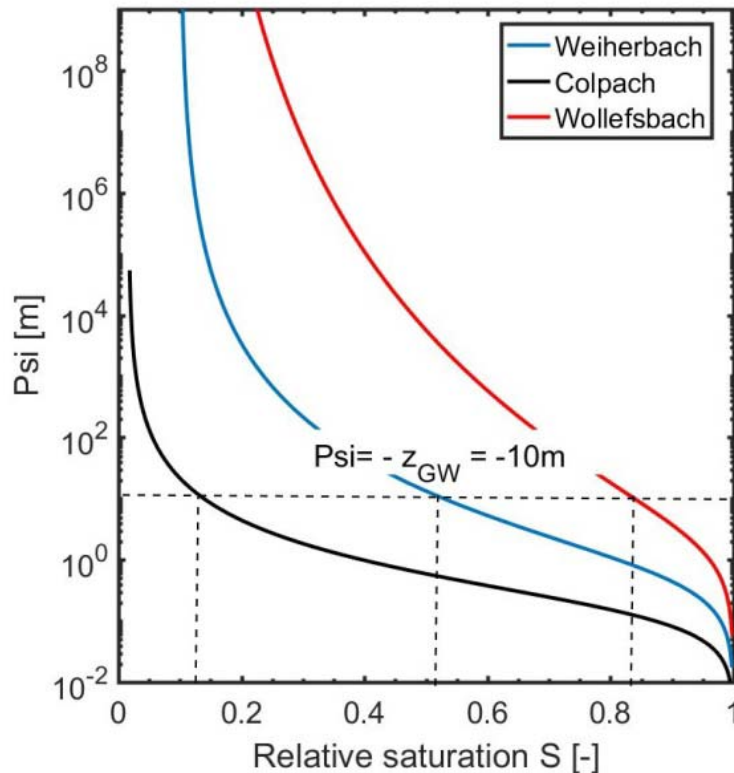
258

$$259 \quad S_{\text{eq}} \equiv \frac{\theta}{\theta_s} \quad |(\psi = -z) \text{ Eq. (7)}$$

260

261 Where  $\theta_s$  ( $\text{m}^3\text{m}^{-3}$ ) is the saturated soil water content and  $S$  (-) is the relative saturation. This is  
262 illustrated in figure 1 for the retention curves of three distinctly different soils.

263



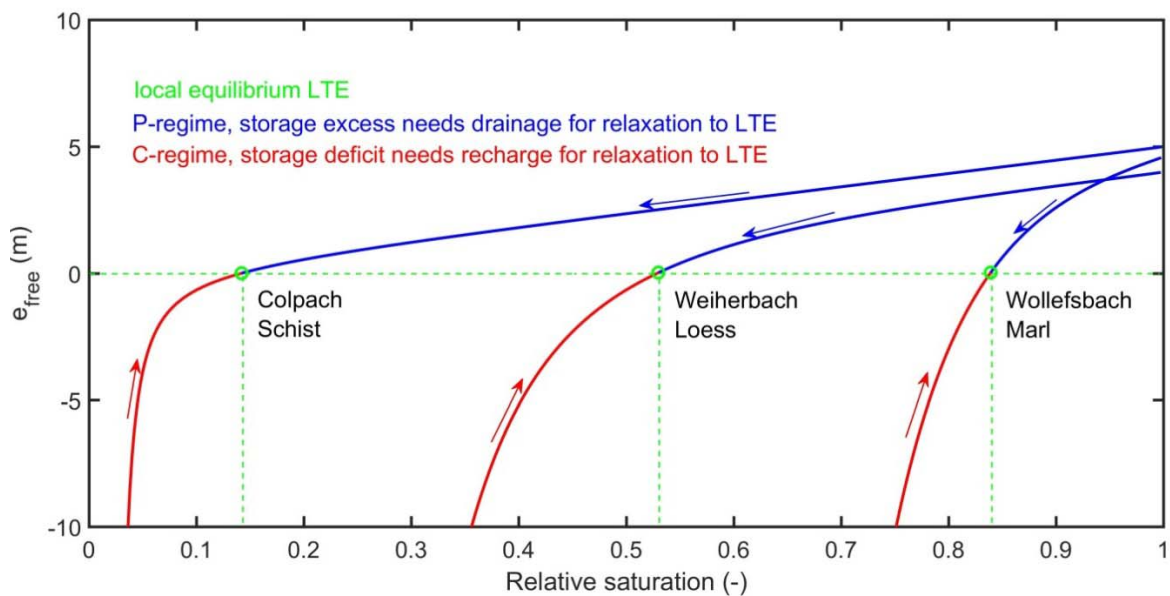
264

265 Figure 1: Soil water retention curves as function of relative saturation determined as explained in  
266 section 3.1. The dashed black lines mark the relative saturation at hydraulic equilibrium, assuming  
267 arbitrarily a depth to groundwater of  $z_{\text{GW}} = 10$  m. The Wollefsbach and the Colpach are further  
268 characterised in section 3.

269 Assuming arbitrarily a depth to groundwater of  $z_{GW} = 10$  m in Eq. (7), leads to very different  
 270 equilibrium saturation values. The equilibrium saturation of the clay rich soil in the Marl  
 271 geological setting of the Wollefsbach catchment is with  $S_{eq} = 0.82$  rather large, while the  
 272 young silty soil located in the Colpach has a rather small saturation at equilibrium of  
 273  $S_{eq} = 0.13$ . The loess soil from the Weiherbach is with  $S_{eq} = 0.53$  in between these extremes.  
 274 Note that two of those soils are located in our respective study areas Colpach and Wollefsbach  
 275 located in Luxembourg (compare section 3). We added the in Germany located Weiherbach  
 276 soil to complete the spectrum of possible endmembers. Although these values are very  
 277 different in magnitude, they represent the respective equilibrium states, which these systems  
 278 at this elevation will naturally approach when relaxing from external disturbances.

### 279 2.3 Free energy state as function of relative saturation

280 The equilibrium storages shown in figure 1 separate furthermore ranges of relative saturation  
 281 where the corresponding free energy of the soil water is either negative or positive. This  
 282 becomes obvious when plotting the specific free energy per unit volume  $e_{free}$  (m) of the soil  
 283 water content at the same elevation above groundwater as function of the relative saturation  
 284 for these soils (Fig. 2).



285  
 286 Figure 2: Weight specific free energy state of the soil water stock, as defined in Eq. (8), plotted against  
 287 the relative saturation of the three different soils, assuming a depth to groundwater of 10m. The green  
 288 lines mark the local equilibrium state where the absolute value of the specific free energy is zero and  
 289 the corresponding equilibrium saturations. Free energy in the P-regime and C-regimes are plotted in  
 290 solid blue and red respectively, the arrows indicate the way back to equilibrium.

292

293 
$$e_{\text{free}} \equiv \frac{g_{\text{free}}}{\rho g} \equiv (\psi(\theta) + z) \cdot \theta = f(S | z = \text{const}) \text{ Eq. (8)}$$

294 Note  $e_{\text{free}}$  is, as being defined as specific free energy per unit volume, equal to the product of  
295 total hydraulic potential and the soil water content. Note that we assume the soil to be in  
296 capillary contact with groundwater (see section 5.2 for further discussion). The horizontal  
297 green line in figure 2 marks the local equilibrium where the absolute value of the specific free  
298 energy at this particular elevation is zero. The vertical lines indicate the corresponding  
299 equilibrium saturations at the x-axis (corresponding to those in figure 1). These equilibrium  
300 storages separate the ranges of soil saturation where the corresponding free energy is positive  
301 (in blue). This is the case as the potential energy is larger than the capillary binding energy;  
302 we call this range the P-regime. In this regime dynamic in soil water content are dominantly  
303 driven by differences in potential energy and gravity dominates. Relaxation back to  
304 equilibrium requires the release of water to deplete the excess in potential energy, and the  
305 necessary amount is determined by the overshoot of free energy above zero.

306 Relative saturations smaller than  $S_{\text{eq}}$  are associated with negative free energy, as the absolute  
307 value of the capillary binding energy exceeds potential energy. We call this range the C-  
308 regime (in red) because differences in capillary binding energy and thus capillarity act as  
309 dominant driver for soil water dynamics. The system needs to recharge water to deplete the  
310 “energy deficit” below zero, and the necessary amount depends on the distance to  
311 equilibrium. Be aware that particularly small changes in soil water content may, depending on  
312 the size of  $\theta d\psi/d\theta$ .

313 Figure 2 depicts that the three different soils, when being arranged at the same geopotential  
314 level, are characterized by distinctly different energy state curves as function of relative  
315 saturation. The P-regime is very prominent for the Colpach soil – potential energy dominates  
316 over a wide range of saturation its  $e_{\text{free}}$  grows linearly with  $S$  for values larger than 0.2. The  
317 clay rich soil of the Wollefsbach has a diametrical pattern, capillarity dominates the energy  
318 state for 82% of the possible saturations and the absolute value of  $e_{\text{free}}$  grows in a strongly  
319 nonlinear way with declining saturation. The energy state function of the loess soil is in-  
320 between the other two extremes with an equilibrium at a saturation of 0.53%.

321 Due equation Eq. (8) the energy state functions shown in figure 2 depend on the soil water  
322 retention curve and the depth above groundwater. While depth to groundwater is usually not  
323 exactly known, height over the next drainage (HAND, Renno et al., 2008; Nobre et al., 2011)

324 provides an easy to measure surrogate when taking the water level of the closest stream as  
325 reference. While depth to groundwater grows obviously proportionally to HAND, the related  
326 proportionality factor  $c$  is not straightforward to calculate. For draining rivers,  $c$  is less or  
327 equal to one, the minimum is expected to be in the order of 0.8, and  $c$  may increase with  
328 increasing distance to the river, reflecting the topography of the groundwater surface. In  
329 addition, the proportionality changes dynamically in response to the spatio-temporal pattern  
330 of groundwater recharge, the hydraulic properties of the aquifer, topography of an aquitard,  
331 and the water level in the stream. Yet we may in characterize the upper limit of free energy  
332 states of root zone soil water storages in a stratified manner by a ‘family’ of energy state  
333 curves, if we know: a) the retention functions of the soils, and b) the frequency distribution of  
334 HAND  $h(z_{\text{HAND}})$  in the system of interest.

335 This family of curves characterizes how HAND and soil physical characteristics jointly  
336 control the free energy state of soil water as function of the relative saturation. The  
337 presentation of the energy state functions for our study areas in the following section 3 will  
338 reveal that all points in the root zone with the same soil water retention curve and which fall  
339 into the same bin of HAND are represented by the same energy state curve.

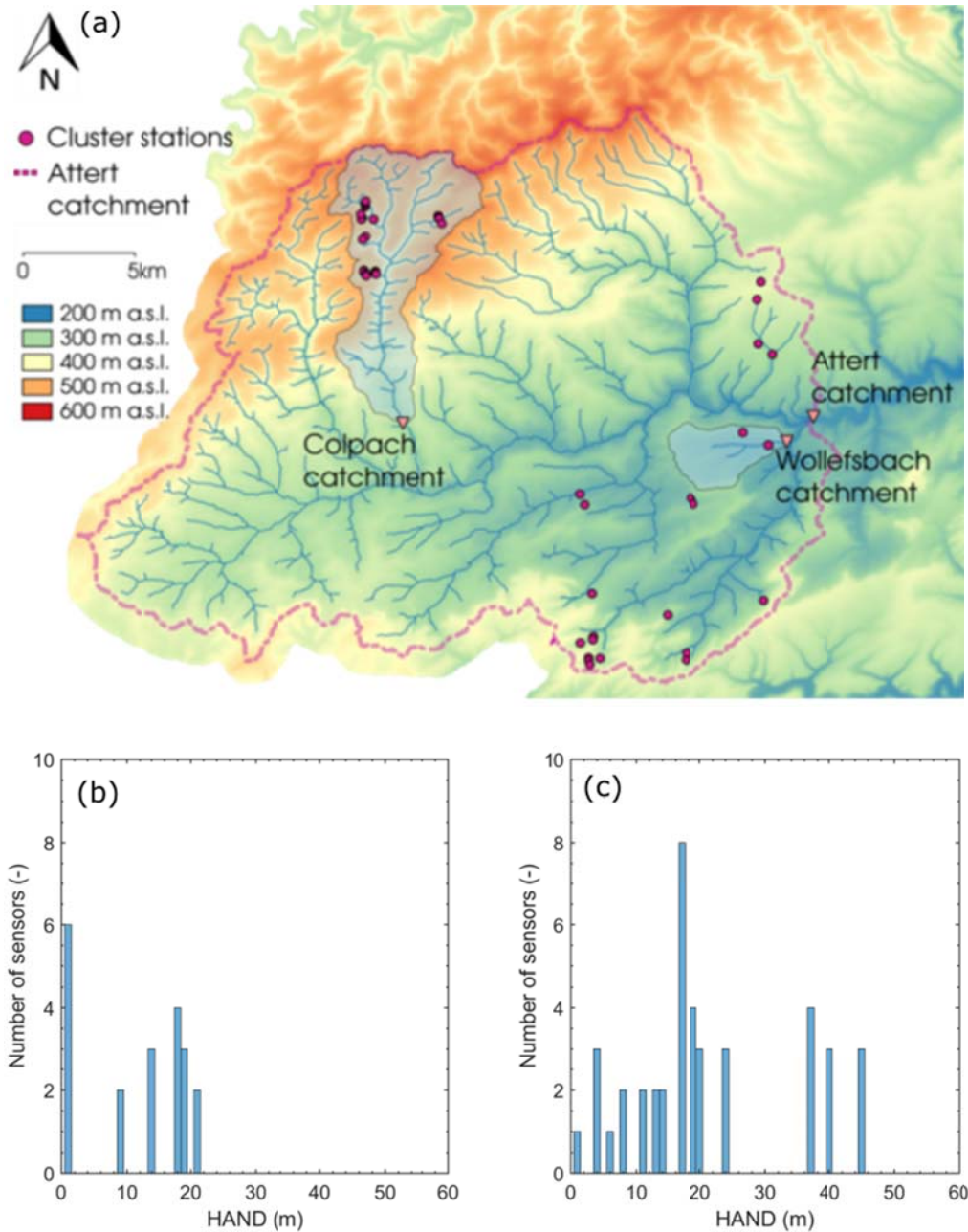
### 340 **3 APPLICATION**

341 The derived energy state function introduced in the last section defines the possible energy  
342 states of the soil water stock, a thermodynamic state space of the root zone so to say. Due to  
343 the intermittent rainfall and radiative forcing, their respective annual cycles, the free energy  
344 state of soil water will be pushed and pulled through this state space. It appears thus  
345 straightforward to visualize these storage dynamics, either observed or modeled, as pseudo  
346 oscillations of the corresponding free energy state in the respective energy state functions.  
347 This will teach us a) which part of the state space is actually visited by the system, and b)  
348 whether the system predominantly operates in one of these regimes or within both them. In  
349 the following, we briefly characterize the study areas and the dataset we use for this purpose.

#### 350 **3.1 Study areas**

351 The Colpach and the Wollefsbach catchments belong to the Attert experimental basin (Pfister  
352 et al., 2002; Pfister et al., 2017), and are distinctly different with respects to soils, topography,  
353 geology and landuse (Fig. 4). Both catchments have been extensively characterized in  
354 previous studies with respect to their physiographic characteristics, dominant runoff  
355 generation mechanisms and available data (Wrede et al., 2015; Martinez-Carreras et al., 2015;

356 Loritz et al., 2017; Angermann et al., 2017). Hence, we focus here exclusively on those  
 357 system characteristics which determine their respective energy state functions. The Colpach  
 358 has an elevation range from 265 to 512 m.



359  
 360 Figure 3: Map of the Atert basin with the Colpach and Wollefsbach catchments (Panel a, taken from  
 361 Loritz et al. 2017). The red dots mark the cluster sites of the CAOS research unit, which collect  
 362 besides the standard hydro-meteorological data, soil moisture and the soil water potential. Panels b and  
 363 c show the distribution of the sensors along HAND for the Wollefsbach and Colpach, respectively.

364 Soils are young silty haplic Cambisols that formed on schistose periglacial deposits. Despite  
 365 of their high silt content they are characterized by a high permeability and high porosity

366 (Jackisch et al., 2017), because the fine silt aggregates embed a fast draining network of  
367 coarse inter-aggregate pores. In contrary, the Wollefsbach has a much more gentle topography  
368 from 245 to 306 to m.a.s.l. Soils in this marl geological setting range from sandy loams to  
369 thick clay lenses.

### 370 **3.2 Storage data, soil water characteristics and energy state functions**

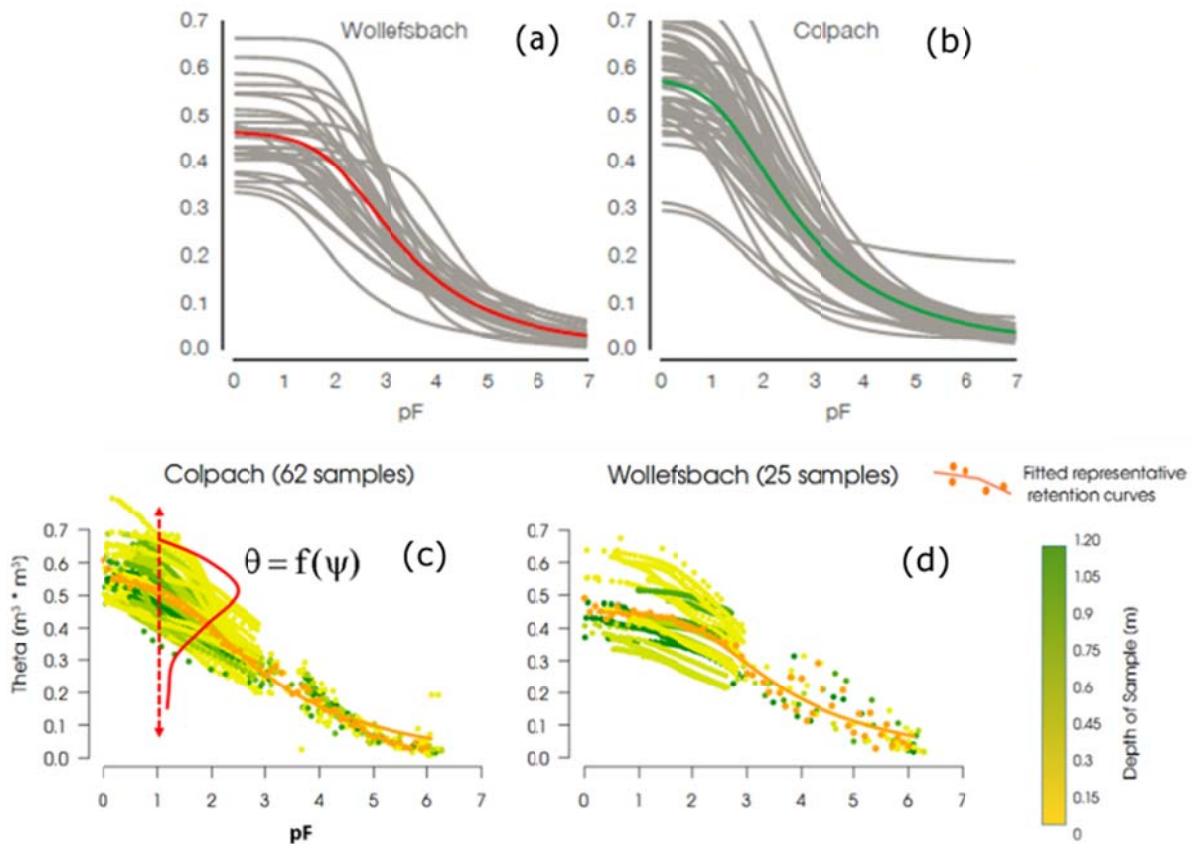
371 For this study, we use data from a distributed network of 45 sensor clusters spread across the  
372 entire Attert experimental basin (Fig. 3) collected within the hydrological year 2013/14. These  
373 clusters measure, among other variables, soil moisture and matric potentials within three  
374 replicated profiles in 0.1, 0.3 and 0.5 m depths using Decagon 5TE capacitive soil moisture  
375 sensors. In this application we focus on data collected in 0.1 m depth, the distributions of  
376 sensors along HAND in the Wollefsbach and the Colpach are shown in figure 3 b and c  
377 respectively. Note that we use HAND as an estimator for the depth to groundwater here. Soil  
378 water retention was in both catchments analyzed by Jackisch (2015) using a set of 62  
379 undisturbed soil cores from the Colpach and 25 undisturbed soil cores from the Wollefsbach  
380 (Figure 4 a and b).

381 Here we do not use these point relations but representative, macroscale soil water retention  
382 functions to derive the energy state function of our study areas (Fig. 4 c and d). These were  
383 derived by Jackisch (2015) from the raw data of all experiments as follows. He pooled the  
384 matching pairs of soil water content and matric potential of all experiments in a landscape into  
385 a single sample (Fig. 5 c and d). When using the tension ( $pF = \log_{10}(-\psi)$ ) as independent  
386 variable, we interpret the corresponding soil water contents of the 62 or 25 experiments as  
387 conditional random variable. The sample reflects the heterogeneity of the soil and needs to be  
388 characterized by a conditional frequency distribution  $h(\theta | \psi)$ . And the latter needs in turn to  
389 be characterized by its moments and percentiles. The averaged soil water content at each  
390 matric potential/tension-level  $\bar{\theta}(\psi)$  is an estimator to the expectation value of the soil water  
391 content at this tension.

392 We define the representative retention curve as the one that relates the expected soil water  
393 storage to the matric potential  $\bar{\theta}=f(\psi)$  and the latter may be obtained by fitting a suitable  
394 retention function to the data, we used the van Genuchten model here (Jackisch, 2015). Note  
395 that this relation cannot be observed at a single site. It is an effective macroscale retention  
396 function characterizing the relation between the expected soil water content in the landscape  
397 and the matric potential, reflecting random distribution  $h(\theta | \psi)$ .

398

399



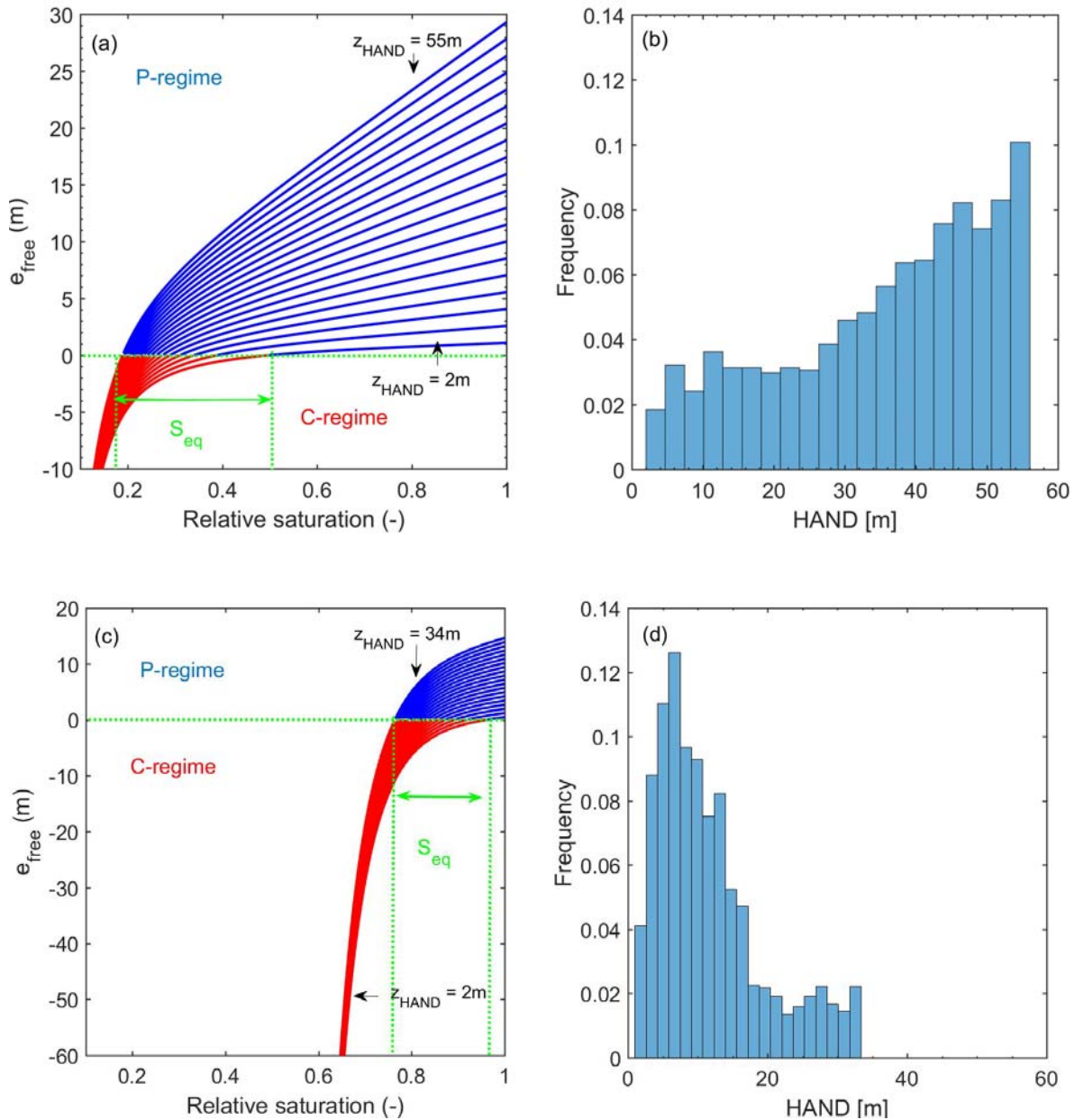
400

401 Figure 4: Panel a and b show the retention functions Jackisch (2015) derived from individual soil cores  
402 by means of multistep outflow experiments. Panels c and d illustrate the procedure of pooling the soil  
403 water contents observed at given tension ( $pF = \log_{10}(\psi)$ ) of all experiments into conditional random  
404 samples. The orange points mark the averaged  $\bar{\theta}$  values as function of the tension and the solid lines  
405 are the mark fitted van Genuchten functions. Note that these representative curves are shown in color  
406 in panel a and b as well. The color code of the individual data points in panel c and d relates to the  
407 depth of the sample below surface.

408 Loritz et al (2017, 2018) used these effective retention functions for setting up physically-  
409 based hydrological models for both catchments, which yielded simulations of stream flow and  
410 soil moisture dynamics in good accordance with observations. Test simulations with  
411 randomly selected retention functions of individual experiments (Fig. 4 b) and based on the  
412 averages of the van Genuchten parameters of 62 experiments performed clearly worse.

413 Based on these representative retention functions and the frequency distributions of HAND  
414 (Fig. 5 b and d) we compiled the energy state functions of both catchments (Fig. 5 a and c)  
415 according to Eq. 8, thereby using HAND as surrogate for the depth to groundwater. As stated

416 in the previous section, the energy state function consists of a family of curves, which  
 417 characterize the free energy state of the soil water as function of the relative saturation,  
 418 stratified along the bin centroids of the corresponding frequency distributions of HAND.



419

420

421 Figure 5: Energy state functions of the Colpach (a) and the Wollefsbach (c) derived from the  
 422 corresponding frequency distributions range of HAND (panels b and c) and the representative  
 423 retention functions (note the differences in scales). The horizontal green line mark the equilibrium of  
 424 zero free energy, the vertical green lines mark the corresponding ranges of equilibrium saturations.  
 425 Please note that  $e_{free}$  at a relative saturation of 1 equals the product of HAND and the soil water content  
 426 at saturation.



427 Note that the wider HAND range in the Colpach causes a clear dominance of the P-Regime  
428 over a large saturation range. More importantly, figure 5a reveals that for relative saturations  
429 larger than  $\sim 0.4$  free energy is a multilinear function of relative saturation. This means that the  
430 specific free energy density is at each HAND level a linear function of relative saturation, but  
431 the slope of the energy state curves does increase with increasing HAND. The corresponding  
432 range of equilibrium saturations is between 0.18 and 0.5. The absolute values of  $e_{\text{free}}$  are in the  
433 corresponding C-regime less than 20m. In the root zone of the Wollefsbach free energy is  
434 contrarily a strongly non-linear function of relative saturation (fig. 5c). The C-regime is very  
435 prominent and  $e_{\text{free}}$  drops below  $-100$  m for saturations smaller than 0.6. This mainly due to  
436 the high clay content in the soil and to a lesser degree it also reflects the smaller HAND in this  
437 landscape. Consistently, we find the ranges of equilibrium saturation between 0.78 and 0.98.

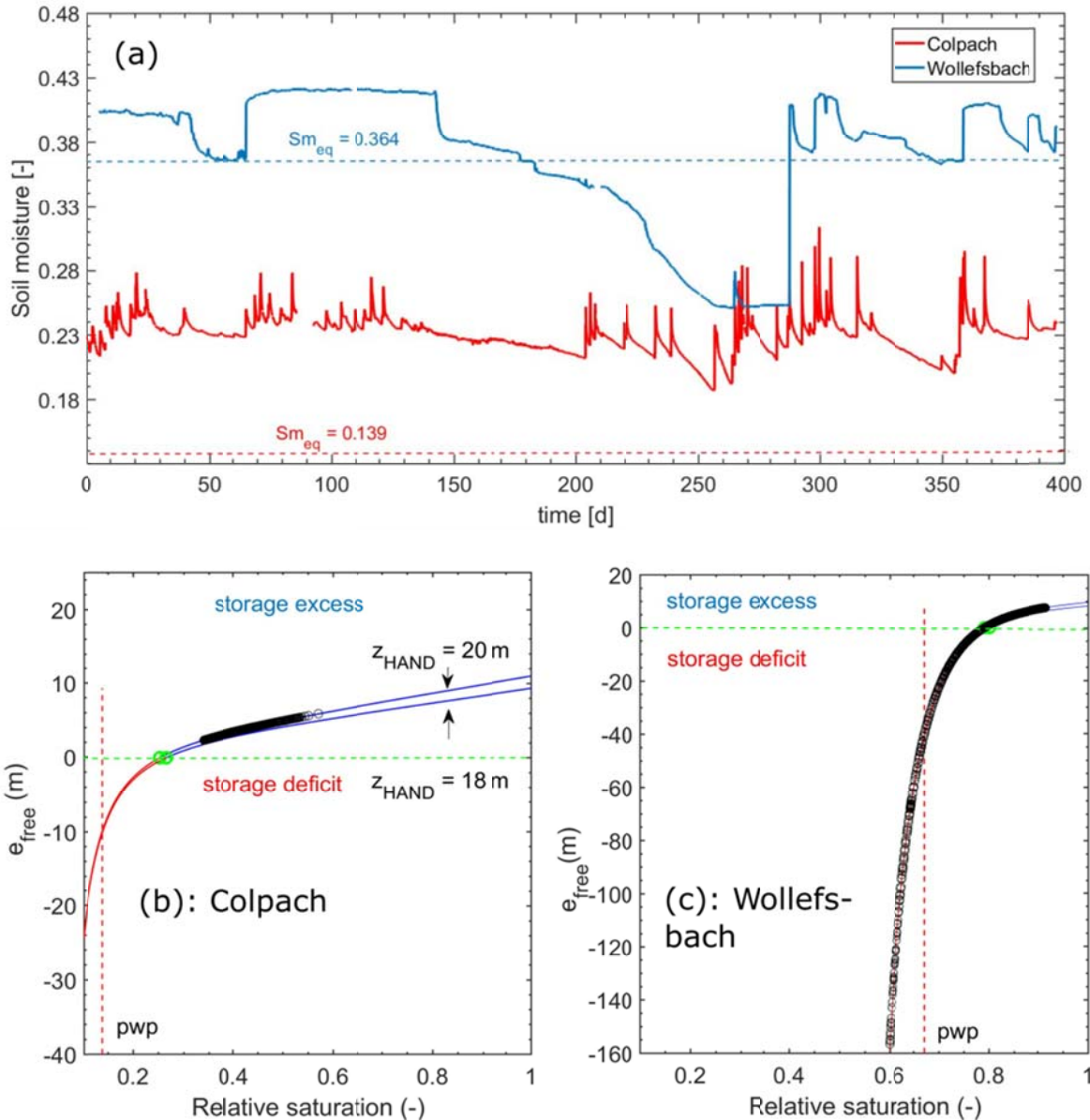
## 438 **4 RESULTS**

### 439 **4.1 Soil moisture and its free energy state at two distinct cluster sites**

440 In a first step we inter-compare the free energy states of the soil moisture stock (Fig. 6) which  
441 was observed at two arbitrarily selected sites in the respective study catchments. Both sites are  
442 located 20 m above their respective streams. The soil water content in the clay rich top soil of  
443 the Wollefsbach site is in the winter and fall period rather uniform and on average  $0.15 \text{ m}^3 \text{ m}^{-3}$   
444 larger than in the Colpach (Fig. 6a). While the soil water content at the Colpach site appears  
445 much more variable in these periods. Both sites dry out considerably during the summer  
446 period and start to recharge with the beginning of the fall. Figure 6a depicts furthermore that  
447 the site in the Colpach operates clearly above the corresponding equilibrium soil water  
448 content,  $\theta_{\text{eq}} = 0.139 \text{ m}^3 \text{ m}^{-3}$ , while the site in the Wollefsbach drops below its equilibrium soil  
449 water content,  $\theta_{\text{eq}} = 0.364 \text{ m}^3 \text{ m}^{-3}$ , and operates in the C-regime for almost 3 months.

450 Figure 6 b and c provide the corresponding free energy states of both soil water time series as  
451 function of the soil saturation. Observations are shown as black circles and the related  
452 theoretical energy state curves, calculated after Eq. 8 are in blue. The first thing to note is that  
453 the observed free energy states for both sites scatter nicely around the theoretical curves.  
454 More interestingly one can see that the spreading of the free energy state of the soil water  
455 stock is at both sites distinctly different. The free energy state of soil water at the Colpach site  
456 is during the entire hydrological year in the P-regime and hence subject to an overshoot in  
457 potential energy (Fig. 6b). The site operates in the linear range of the energy state curve and  
458 fluctuates around an average weight specific energy density of 3.2 m, which corresponds to an

459 energy density of  $2.9 \cdot 10^4 \text{ Jm}^{-3}$ . While the observations spread across a total range of 3 m ( $2.9$   
 460  $10^4 \text{ Jm}^{-3}$ ) their standard deviation is 0.44 m ( $3.0 \cdot 10^3 \text{ Jm}^{-3}$ ). The coefficient of variation of the  
 461 free energy state of the soil water content is hence with 0.14 rather small.  
 462



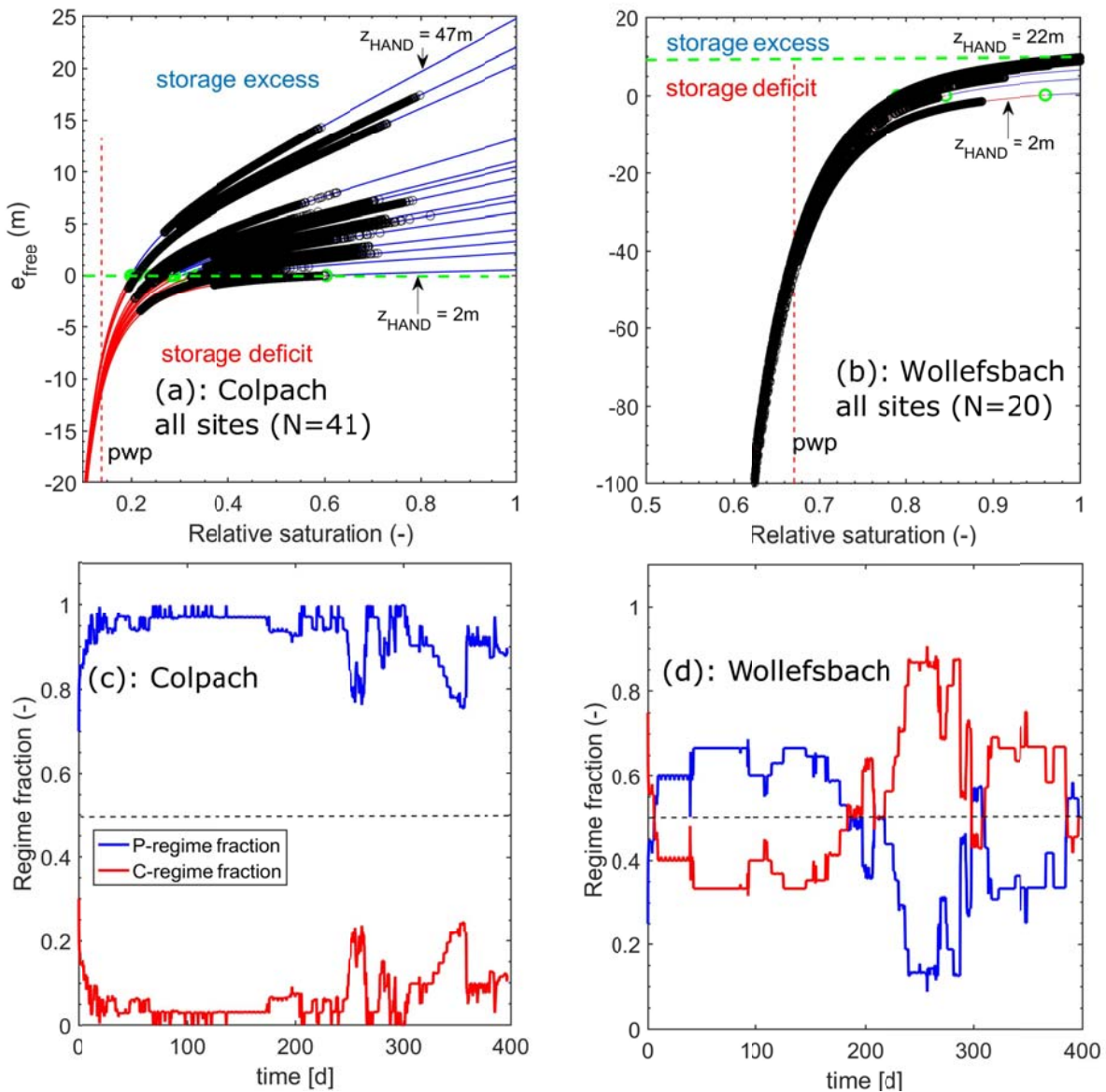
463  
 464 Figure 6: Top soil water content observed at cluster sites in the Colpach and the Wollefsbach  
 465 catchment (panel a) and the corresponding free energy states in their respective energy state curves  
 466 (panel b and c note the different scaling of the ordinates). The black circles mark the observations. The  
 467 vertical dashed line marks the permanent wilting point, which is due to the definition of the total free  
 468 energy in Eq. 8 not simply equal to a total hydraulic potential of -133 m. Panels b and c show  
 469 additionally the energy state curve when contamination the real value with an error of 2 m ( $z_{HAND} =$   
 470 18 m). This is to highlight that an error in the estimated depth to groundwater implies a substantial  
 471 mismatch between observations and the theoretically predicted curve.  
 18

472 In the Wollefsbach the weight specific free energy density of soil water spreads across a much  
473 wider range of almost 180m, which corresponds to  $1.79 \cdot 10^6 \text{ Jm}^{-3}$  (Fig. 6c). The average  
474 specific free energy density is with  $-44.3 \text{ m}$  ( $-4.41 \cdot 10^5 \text{ Jm}^{-3}$ ) strongly negative, the  
475 distribution is highly skewed towards the negative value and the coefficient of variation is  
476 with 2.8 much larger. Most importantly the system operates qualitatively differently as it  
477 switches to the C regime during the dry spell in the summer period and stays there for nearly  
478 three months. Please note that the free energy declines to the values which are clearly below  
479 the permanent wilting point pwp. (As specific free energy is the product of the total soil  
480 hydraulic potential and the soil water content, its value at the pwp does not simply correspond  
481 to  $-133\text{m}$ ). To understand this strong decline in soil water content it is important to recall that  
482 drying of the top 0.1 m of the soil, is strongly influenced by evaporation and that the water  
483 potential of unsaturated air is at a relative humidity of 90% clearly below the permanent  
484 wilting point (Porada et al., 2011).

485 We hence state that the free energy state of the soil water stock reveals a distinctly different  
486 dynamic behavior of both sites, which cannot be derived from the comparison of the  
487 corresponding soil water moisture time series. The Colpach site is characterized by permanent  
488 storage excess, though the corresponding soil water content is always smaller than in the  
489 Wollefsbach. Free energy of the soil water stock is in this range a linear function of relative  
490 saturation. This implies that the energy difference which dominantly drives soil water  
491 dynamics changes linearly with soil water content, or in other terms gravity potential  
492 dominates against matric potential. The retention function in Figure 1 shows that the matric  
493 potential in the Colpach is at the minimum observed saturation of  $S=0.3$  (Figure 6b) equals  $-2 \text{ m}$ .  
494 This implies according to Eq. 8 that  $e_{\text{free}} = -0.3 \cdot \theta_s 2\text{m} + 0.3 \cdot \theta_s 20 \text{ m} = 2.91 \text{ m}$  and that potential  
495 energy is 10 times larger than capillary binding energy. For larger saturations the first term  
496 remains rather constant while the second grows linearly with saturation. In contrary, the  
497 Wollefsbach shows a strongly non-linear behavior at this site and it switches to a storage  
498 deficit when the soil saturation drops below 0.79 (Fig. 6a). In a further step we contaminated  
499 the HAND values of both sites with an error of 2m and plotted the corresponding energy state  
500 curves ( $z_{\text{HAND}} = 18 \text{ m}$ ). This curve does considerably mismatch the observations (Figure 6b, c).  
501 This corroborates a) that HAND is a good estimator of depth to groundwater at this point and b)  
502 that an error in the estimated depth to groundwater leads to a mismatch between the theoretical  
503 energy state curve and the observed values. This implies that the observed energy states will  
504 also change with changing groundwater surface, as further detailed in the discussion.

505 **4.2 Soil moisture and its free energy state within the entire observation**  
 506 **domain**

507 Figure 7 presents the free energy states of the soil moisture which was observed at all cluster  
 508 sites in the Colpach (panel a, N = 41) and the Wollefsbach (panel b, N = 20). The respective  
 509 heights above the channel range from 1 to 45 m in the Colpach and from 1 to 22m in the  
 510 Wollefsbach (Fig. 3 b and c).



511  
 512 Figure 7: Free energy of all observations in the Colpach (a) and Wollefsbach (b) plotted in their  
 513 corresponding energy state function (note the different scales). The black circles mark the  
 514 observations. The horizontal green lines mark the equilibrium of zero free energy. Panel c and d show  
 515 which fractions of the data set was in the P or in the C regime as function of time. Note that the  
 516 corresponding distributions of HAND are shown in Figure 3 b and c.  
 517

518 Generally, the observed free energy states scatter again nicely around the energy state curves  
519 of the corresponding HAND. The Colpach operates except for a few sites most of the time in  
520 the linear range of the P-regime, indicating that soil moisture dynamics is dominated by  
521 potential energy differences. Observations in the Colpach generally spread across a wide  
522 range of relative saturations, and the corresponding “amplitudes” of the free energy deviations  
523 are clearly larger as at the single site shown in Figure 6 b. This is because sensor clusters with  
524 the same HAND were pooled into the same subsample regardless of their separating distance.  
525 For instance, at  $z_{\text{HAND}} = 1$  m the subsample consisted of 1 cluster with three replicate soil  
526 moisture profiles, at  $z_{\text{HAND}} = 17$  we had for instance 3 sensor clusters and thus in total 8 soil  
527 moisture profiles. The partly large spreading of the observations may hence be explained by a  
528 combination of local scale heterogeneity and large scale differences in the drivers of soil  
529 water dynamics such as rainfall or local characteristics of forest vegetation.

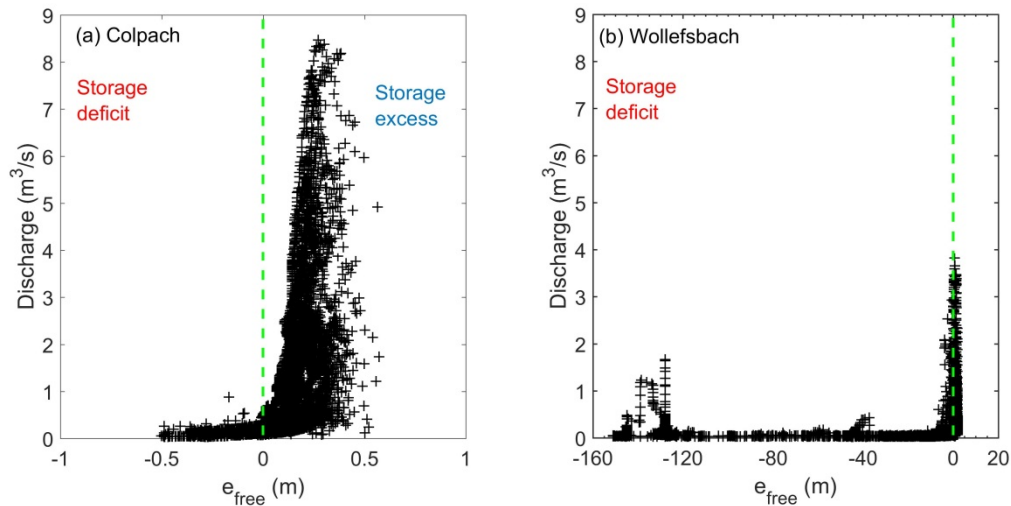
530 Despite of the large spreading, 80% of the Colpach sites operated permanently in the P-  
531 Regime (Fig. 7c). During the wet season it is more than 90 % of the sites, between day 250  
532 and 400, quite a few profiles switch into the C-regime and thus to a storage deficit. These  
533 profiles are mostly located at the smallest heights over the next drainage, while only some of  
534 those are at a larger HAND of 37 m and 22 m.

535 In the Wollefsbach we find, consistently with figure 7b, a clear drop of free energy into the C-  
536 regime during the dry spell in the summer period. All sites drop clearly below the permanent  
537 wilting point, which corroborates the strong evaporative drying of the top soil in this  
538 landscape. In contrary to the Colpach, the fractions of profiles which operate in the different  
539 regimes are much more variable in time (Fig. 7d). During the observation period, on average  
540 50% of the profiles operate in the C-regime and thus a storage deficit. The minimum is 30%  
541 and the C-regime fraction peaks at 90% at day 250. Note that more than 50% of the sites are  
542 continuously in the C-regime during the second half of the observation period. These  
543 differences are consistent with the strongly different runoff generation behavior of both  
544 systems, as further detailed in the next section.

### 545 **4.3 Free energy state as control of stream flow generation**

546 An interesting question is whether the free energy state of the soil water content and  
547 particularly the separation of the C- and the P-regimes is helpful to explain the onset of  
548 storage controlled stream flow generation in both landscapes. As storage controlled runoff  
549 response to rainfall is not generated everywhere in the catchment but mostly in the riparian  
550 zone, the energy state of soil water at large values HAND is pretty unimportant in this respect.

551 We thus plotted for the entire hydrological year the observed streamflow in both catchments  
 552 against the energy state of soil water for sites at the smallest HAND values of 2m which are  
 553 close to the riparian zone (Figure 8 a and b).



554  
 555 Figure 8: Observed stream flow in the Colpach (Panel a, drainage area is 19.2 km<sup>2</sup>) and the  
 556 Wollefsbach (Panel b, drainage area is 4.5 km<sup>2</sup>) plotted against the free energy of sites in their  
 557 corresponding riparian zones.

558 Both scatter plots reveal distinct threshold like dependence of streamflow on the free energy  
 559 state of soil water and note that the threshold coincides with the state of zero free energy,  
 560 which separates the C- from the P-Regime. Streamflow in the Colpach is rather uniform, if the  
 561 riparian zone is with respect to the local equilibrium in a storage deficit (Fig. 8a), while  
 562 streamflow shows a strong variability when the system switches to a storage excess in the P-  
 563 regime. The transition to a state of storage excess, which implies that the system needs to  
 564 release water to relax back to local equilibrium, coincides with the onset of storage controlled  
 565 streamflow generation. The variability of streamflow in P-regime does of course also reflect  
 566 the variability in the rainfall forcing. Streamflow in the C-Regime likely feeds exclusively  
 567 from groundwater. This behavior is pretty much consistent with our theoretical expectation.

568 In the Wollefsbach we observe a slightly different pattern. On the one hand there is a similar  
 569 sharp increase of streamflow when free energy of soil water in the riparian zone switches  
 570 from the C- to the P-regime. On the other hand one may observe distinct values of stream  
 571 flow for specific free energy densities of in the range between -1m and 10m, at -40 m and  
 572 below -120 m. This reflects infiltration excess runoff generation, which is frequently observed  
 573 in this Marl setting, as these states correspond to unsaturated hydraulic conductivities of either  
 574  $5 \cdot 10^{-7}$  m/s or  $1 \cdot 10^{-9}$  m/s or even smaller values. Although overland flow also occurs in the

575 Colpach, it only occurs on compacted forest roads, but not in the riparian zone or in upslope  
576 pristine areas.

## 577 **5 DISCUSSION AND CONCLUSIONS**

578 The presented results provide clear evidence that a thermodynamic perspective on soil water  
579 storage provides holistic information for judging and inter-comparing soil water dynamics,  
580 which cannot be inferred from soil moisture observations alone. In the following we reflect  
581 the general idea of using free energy as state measure, discuss its promises as well as its  
582 limiting assumptions. We then move on to the more specific differences in the storage  
583 dynamics in both studied catchments. And we close by reflecting on the seeming paradox  
584 between the known local non-linearity of soil physical characteristics and the frequent  
585 argumentation that hydrological systems often behave much more linearly.

### 586 **5.1 Free energy and the energy state function – options and limitations**

587 Our results clearly show that free energy as function of relative soil saturation holds the key to  
588 define a meaningful state space of the root zone of a hydrological landscape. This space of  
589 possible energy states consists of a family of energy state curves, where each of those  
590 characterizes how free energy density evolves at a height above the next drainage, depending  
591 on the triad of the matric potential, HAND (i.e. as a surrogate for the unknown gravity  
592 potential) and soil water content. The free energy state of soil water reflects in fact the balance  
593 between its capillary binding energy and geo-potential energy densities and we showed that  
594 this balance determines:

- 595 • Whether a system is at given elevation above groundwater locally in its equilibrium  
596 storage state ( $e_{\text{free}} = 0$ ), in a state of a storage deficit ( $e_{\text{free}} < 0$ ) or in state of a storage  
597 excess ( $e_{\text{free}} > 0$ );
- 598 • The regime of storage dynamics. Soil water dynamics in the C-regime ( $e_{\text{free}} < 0$ ) are  
599 dominated by capillarity i.e. differences in local matric potentials act as dominant  
600 driver. The soil needs to recharge to relax to its local equilibrium. Or it is in the P-  
601 regime ( $e_{\text{free}} > 0$ ) dominated by potential energy, i.e. the non-local linear gravitational  
602 control dominate soil water dynamics, the system needs to release water to relax to  
603 local equilibrium.

604 The energy level function turned out to be useful for inter-comparing distributed soil moisture  
605 observations among different hydrological landscapes, as it shows the trajectory of single sites

606 or of the complete set of observations in its energy state space. This teaches us which part of  
607 the state space is actually ‘visited’ by the system during the course of the year, whether the  
608 system operates predominantly in a single regime, whether it switches between both regimes  
609 during dry spells and how much water needs to be released or recharged locally for relaxing  
610 back to local equilibrium and how often it actually reaches its equilibrium.

611 Note that the usual comparison of soil water contents alone did not yield this information. On  
612 the contrary from this we would conclude that the site in the Wollefsbach is, due to the higher  
613 soil water content, always ‘wetter’ than the corresponding site in the Colpach. The free energy  
614 state reveals, however, the exact opposite, we have a storage excess at Colpach site for the  
615 entire year while the Wollefsbach site is in summer in a storage deficit. We thus propose that  
616 the term wet and dry should only be used with respect to the equilibrium storage as  
617 meaningful reference point.

618 The free energy state of soil water in the riparian zone of both study catchments has  
619 furthermore been proven to be rather helpful to explain the onset of streamflow generation.  
620 We found a distinct threshold behavior for storage controlled runoff production in both  
621 catchments, and clear hints at overland flow contributions in the Wollefsbach. While we  
622 admit that a threshold like dependence of the onset of runoff is frequently reported (Ragan,  
623 1968, Gillham, 1984, McDonnell, 1990, Bishop, 1991, Tromp-van Meerveld et al. 2006) we  
624 like to stress that the tipping point we found here has a theoretical basis. In both areas it  
625 coincides with local equilibrium state of zero free energy – the onset of a potential energy  
626 excess of soil water in the riparian zone coincides with the onset of storage controlled  
627 streamflow generation.

628 The apparent strong sensitivity of the free energy state of soil water to the estimated depth to  
629 groundwater, offers on new opportunities for data based learning and an improved design of  
630 measurement campaigns, but it also determines the limits of the proposed approach. With  
631 respect to the first aspect, we could show that an error of 2 m in the assumed depth to  
632 groundwater lead to a clear deviation of the observed free energy states from the theoretical  
633 energy level curve. This offers either the opportunity to estimate depth to groundwater from  
634 joint observations of soil moisture and matric potential, in case the local retention function is  
635 known. This can, for instance, be done by minimizing the residuals between the observation  
636 and the theoretical curve as function of depth to groundwater. Or it allows for the derivation  
637 of a retention function based on the joint observations of soil moisture, matric potential and  
638 depth to groundwater. Here, we need again to minimize the residuals between the observation



639 and the theoretical curve but this time as function of the parameters of the soil water retention  
640 curve. Due to this strong sensitivity it is furthermore important to stratify soil moisture  
641 observations both according to the installed depth of the probe and according to the elevation  
642 of the site above groundwater, or the height over the next stream. The latter is important  
643 because depth to groundwater determines the equilibrium storage the site will approach when  
644 relaxing from external forcing.

645 Despite of all these opportunities for learning, the sensitivity of free energy to the estimated  
646 depth to groundwater implies that the site of the system is still in hydraulic contact with the  
647 aquifer. This key assumption is certainly violated if the soil gets so dry that the water phase  
648 becomes immobile while the air phase becomes the mobile phase. And it might get violated if  
649 depth to groundwater becomes too large. Last but not least the groundwater surface may  
650 change either seasonally, or in some systems more rapidly, and this might imply step changes  
651 in the energy state function and the storage equilibrium.

652 We nevertheless conclude that it is worth to collect joint data sets either of the triple of soil  
653 moisture, matric potential and the retention function at distributed locations (as we did in the  
654 CAOS research unit as explained in (Zehe et al. 2014)) or even preferable on the quadruple of  
655 soil moisture, matric potential, retention function and depth to groundwater. Soil moisture  
656 observations alone appear not very informative about the system state. This is because they do  
657 neither tell anything about the binding state of water, nor about how the system deviates from  
658 its equilibrium and which process is “needed” to relax.

## 659 **5.2 Storage dynamics in different landscapes – local versus non local** 660 **controls**

661 In line with our proposition we found indeed a distinctly typical interplay between capillary  
662 and gravitational controls on soil water in our study areas, and those were in the Colpach  
663 substantial different compared to the Wollefsbach. The observations clearly revealed that the  
664 top soil in the Colpach operates the entire hydrological year largely in a state of storage  
665 excess due to an overshoot in potential energy. Soil water dynamics is mainly driven by  
666 differences in potential energy, which means that the linear and non-local gravitational control  
667 dominates. Most interestingly we found that the free energy state of the soil operated for a  
668 considerable time of the year in the linear range of the P-regime, which implies that the  
669 storage dynamics is (multi) linear. This means that the specific free energy density is at each  
670 HAND level a linear function of relative saturation, but the slope of the energy state curves  
671 does increase with increasing geopotential. We found furthermore that the annual variation of

672 the averaged free energy of the soil water stock was rather small. Zehe et al. (2013) found a  
673 similar, almost steady state behavior, for the averaged free energy of the soil water stock in  
674 the Mallalcahuello catchment in Chile, which also operated in the P-regime the entire year.  
675 Note that both landscapes are characterized by a pronounced topography, by well drained  
676 highly porous soils (Blume et al., 2008a; Blume et al., 2008b; Blume et al., 2009) and that  
677 both are predominantly forested. In both landscape subsurface storm flow and thus storage  
678 controlled runoff generation is the dominant mechanism of streamflow generation. This is  
679 consistent with our finding that gravity is the dominant control of soil water dynamics.  
680 On the contrary the Wollefsbach was characterized by a seasonal change between both  
681 regimes: operation in the P-regime during the wet season and a drop to a C-Regime and a  
682 storage deficit during the dry summer period. Free energy was at all sites on average negative,  
683 and a non-linear function of the relative saturation. Interestingly we found the same  
684 seasonality for the Weiherbach catchment in Germany, a dominance of potential energy  
685 during the wet season and a strong dominance of capillary surface energy in summer (Zehe et  
686 al 2013). Note that both landscapes are characterized by cohesive soils, more silty in the  
687 Weiherbach and more clay rich in the Wollefsbach, and a gentle topography. And both are  
688 used for agriculture. In both areas Hortonian overland flow would play the dominant role, but  
689 this process is actually strongly reduced due to a large amount of worm burrows acting as  
690 macropores (Zehe and Blöschl; 2004; Schneider et al., 2018) . Both landscapes are also  
691 controlled by tile drains. In both areas the soil water dynamics is dominated by capillarity  
692 during the summer period, which means that the local soil physical control dominates root  
693 zone soil moisture dynamics.

### 694 **5.3 Concluding remarks**

695 Overall we conclude that a thermodynamic perspective on hydrological systems provides  
696 valuable insights helping us to better understand and characterize different landscapes. Given  
697 the strong relation between a potential energy excess of soil water in the riparian zone and the  
698 onset of storage controlled streamflow production we found in our study areas it seems  
699 promising to further explore the value of free energy for hydrological predictions. We also  
700 conclude that it makes sense to use the terms wet and dry only with respect to the equilibrium  
701 storage as meaningful reference point, because the latter determines whether the soil is with  
702 respect to the free energy state in a state of storage excess or a storage deficit. Another key  
703 finding is that the energy level function, which can be seen as a straightforward generalization  
704 of the soil retention function, accounts jointly for capillary and gravitational control on soil

705 moisture dynamics. With this we link the non-linear soil physical control and the  
706 topographical control on storage dynamics in a stratified manner and use HAND as a  
707 surrogate for the gravitational potential. A nice co-lateral finding is that a linear dependence  
708 of free energy on soil saturation does not compromise the non-linearity of soil water  
709 characteristics. In contrary it may be explained by the dominance of potential energy for  
710 catchments with pronounced topography and during not too dry conditions, and this implies  
711 that at least the energy difference driving soil water dynamics is a linear function of the stored  
712 water amount. The latter is the basis of the linear reservoir, which is frequently used in  
713 conceptual modelling. The option for linear behavior of the subsurface is hence not only  
714 inherent to Darcy's law of the saturated zone, as has been shown by de Rooij (2013) by  
715 deriving aquifer scale flow equations for strip aquifers. Even in the top of the unsaturated  
716 zone a linear relation between storage and driving potential energy differences might emerge.  
717 This inherent option for linear behavior is likely the reason why conceptual models, which  
718 usually do not account for soil physical characteristics, work in some catchments very well  
719 and in others they don't. Based on the presented findings one could speculate that conceptual  
720 models work well in system which are dominated by potential energy.

721

722 ACKNOWLEDGMENTS: We sincerely thank both reviewers, particularly Gerrit de Rooij,  
723 for their thoughtful and valuable feedback. This study contributes to and greatly benefited  
724 from the "Catchments as Organized Systems" (CAOS) research unit. We thank the German  
725 Research Foundation (DFG) for funding (FOR 1598, ZE 533/11-1, ZE 533/12-1). The authors  
726 acknowledge support by Deutsche Forschungsgemeinschaft and the Open Access Publishing  
727 Fund of Karlsruhe Institute of Technology (KIT). The service charges for this open access  
728 publication have been covered by a Research Centre of the Helmholtz Association. The code  
729 and the data underlying this study are freely available by email request to the contact author.

## 730 **6 REFERENCES**

- 731 Angermann, L., Jackisch, C., Allroggen, N., Sprenger, M., Zehe, E., Tronicke, J., Weiler, M.,  
732 and Blume, T.: Form and function in hillslope hydrology: Characterization of  
733 subsurface flow based on response observations, *Hydrology And Earth System*  
734 *Sciences*, 21, 3727-3748, 10.5194/hess-21-3727-2017, 2017.
- 735 Beven, K. J.: Searching for the holy grail of scientific hydrology:  $Q_t = (s, r, \delta t)a$  as closure,  
736 *Hydrology and Earth Systems Science*, 10, 609-618, 2006.

- 737 Blume, T., Zehe, E., and Bronstert, A.: Investigation of runoff generation in a pristine, poorly  
738 gauged catchment in the Chilean Andes II: Qualitative and quantitative use of tracers at  
739 three spatial scales, *Hydrological Processes*, 22, 3676-3688, 10.1002/hyp.6970, 2008a.
- 740 Blume, T., Zehe, E., Reusser, D. E., Iroume, A., and Bronstert, A.: Investigation of runoff  
741 generation in a pristine, poorly gauged catchment in the Chilean Andes I: A multi-method  
742 experimental study, *Hydrological Processes*, 22, 3661-3675, 10.1002/hyp.6971, 2008b.
- 743 Blume, T., Zehe, E., and Bronstert, A.: Use of soil moisture dynamics and patterns at different  
744 spatio-temporal scales for the investigation of subsurface flow processes, *Hydrology  
745 And Earth System Sciences*, 13, 1215-1233, 2009.
- 746 Bolt, G. H., and Frissel M. J.: Thermodynamics of soil moisture, *Netherlands journal of  
747 agricultural science*, 8, 57-78, 1960.
- 748 Budyko, M. I.: The heat balance of the earth's surface, U.S. Dept of Commerce, Washington,  
749 1958.
- 750 de Rooij, G. H.: Averaging hydraulic head, pressure head, and gravitational head in  
751 subsurface hydrology, and implications for averaged fluxes, and hydraulic conductivity,  
752 *Hydrology And Earth System Sciences*, 13, 1123-1132, 2009.
- 753 de Rooij, G. H.: Averaged water potentials in soil water and groundwater, and their  
754 connection to menisci in soil pores, field-scale flow phenomena, and simple  
755 groundwater flows, *Hydrol. Earth Syst. Sci.*, 15, 1601-1614, doi: 10.5194/hess-15-  
756 1601-2011, 2011.
- 757 de Rooij, G. H.: Aquifer-scale flow equations as generalized linear reservoir models for strip  
758 and circular aquifers: Links between the Darcian and the aquifer scale, *Water Resour.  
759 Res.*, 49, 8605-8615, doi:10.1002/2013WR014873, 2013.
- 760 Edelfson and Anderson: Thermodynamics of soil moisture, *Hilgardia*, 15, p31, 1940.
- 761 Favis-Mortlock, D. T., Boardman, J., Parsons, A. J., and Lascelles, B.: Emergence and  
762 erosion: A model for rill initiation and development, *Hydrological Processes*, 14, 2173-  
763 2205, 10.1002/1099-1085(20000815/30)14:11/12<2173::aid-hyp61>3.0.co;2-6, 2000.
- 764 Gao, H., Hrachowitz, M., Schymanski, S. J., Fenicia, F., Sriwongsitanon, N., and Savenije, H.  
765 H. G.: Climate controls how ecosystems size the root zone storage capacity at  
766 catchment scale, *Geophysical Research Letters*, 41, 7916-7923, 10.1002/2014gl061668,  
767 2014.
- 768 Graeff, T., Zehe, E., Reusser, D., Lück, E., Schröder, B., Wenk, G., John, H., and Bronstert,  
769 A.: Process identification through rejection of model structures in a mid-mountainous  
770 rural catchment: Observations of rainfall-runoff response, geophysical conditions and  
771 model inter-comparison, *Hydrological Processes*, 23, 702-718, 10.1002/hyp.7171, 2009.
- 772 Hergarten, S., Winkler, G., and Birk, S.: Transferring the concept of minimum energy  
773 dissipation from river networks to subsurface flow patterns, *Hydrology And Earth  
774 System Sciences*, 18, 4277-4288, 10.5194/hess-18-4277-2014, 2014.
- 775 Hildebrandt, A., Kleidon, A., and Bechmann, M.: A thermodynamic formulation of root water  
776 uptake, *Hydrology And Earth System Sciences*, 20, 3441-3454, 10.5194/hess-20-3441-  
777 2016, 2016.
- 778 Howard, A. D.: Theoretical model of optimal drainage networks, *Water Resour. Res.*, 26,  
779 2107-2117, 1990.

- 780 Howard, A. D. Optimal angles of stream junctions: geometric stability to capture and  
781 minimum power criteria. *Water Resour. Res.* 7, 863 -873, 1971.
- 782 Jackisch, C.: Linking structure and functioning of hydrological systems – How to achieve  
783 necessary experimental and model complexity with adequate effort, PhD thesis, KIT  
784 Karlsruhe Institute of Technology, <https://doi.org/10.5445/IR/1000051494>, 2015.
- 785 Jackisch, C., Angermann, L., Allroggen, N., Sprenger, M., Blume, T., Tronicke, J., and Zehe,  
786 E.: Form and function in hillslope hydrology: In situ imaging and characterization of  
787 flow-relevant structures, *Hydrology And Earth System Sciences*, 21, 3749-3775,  
788 10.5194/hess-21-3749-2017, 2017.
- 789 Kleidon, A., and Schymanski, S.: Thermodynamics and optimality of the water budget on  
790 land: A review, *Geophysical Research Letters*, 35, L20404 10.1029/2008gl035393,  
791 2008.
- 792 Kleidon, A., Zehe, E., Ehret, U., and Scherer, U.: Thermodynamics, maximum power, and the  
793 dynamics of preferential river flow structures at the continental scale, *Hydrology And  
794 Earth System Sciences*, 17, 225-251, 10.5194/hess-17-225-2013, 2013.
- 795 Kleidon, A., Renner, M., and Porada, P.: Estimates of the climatological land surface energy  
796 and water balance derived from maximum convective power, *Hydrology And Earth  
797 System Sciences*, 18, 2201-2218, 10.5194/hess-18-2201-2014, 2014.
- 798 Koehler, B., Corre, M. D., Steger, K., Well, R., Zehe, E., Sueta, J. P., and Veldkamp, E.: An  
799 in-depth look into a tropical lowland forest soil: Nitrogen-addition effects on the  
800 contents of n<sub>2</sub>o, co<sub>2</sub> and ch<sub>4</sub> and n<sub>2</sub>o isotopic signatures down to 2-m depth,  
801 *Biogeochemistry*, 111, 695-713, 10.1007/s10533-012-9711-6, 2012.
- 802 Kondepudi, D., and Prigogine, I.: *Modern thermodynamics: From heat engines to dissipative  
803 structures*, John Wiley Chichester, U. K., 1998.
- 804 Lee, H., Sivapalan, M., and Zehe, E.: Representative elementary watershed (rew) approach, a  
805 new blueprint for distributed hydrologic modelling at the catchment scale: The  
806 development of closure relations, in: *Predicting ungauged streamflow in the mackenzie  
807 river basin: Today's techniques and tomorrow's solutions*, edited by: Spence, C.,  
808 Pomeroy, J., and Pietroniro, A., Canadian Water Resources Association (CWRA),  
809 Ottawa, 165-218, 2005.
- 810 Lee, H., Zehe, E., and Sivapalan, M.: Predictions of rainfall-runoff response and soil moisture  
811 dynamics in a microscale catchment using the crew model, *Hydrology And Earth  
812 System Sciences*, 11, 819-849, 2007.
- 813 Leopold, L. B., and Langbein, W. L.: The concept of entropy in landscape evolution, U.S.  
814 *Geol. Surv. Prof. Pap.*, 500-A, 1962.
- 815 Loritz, R., Hassler, S. K., Jackisch, C., Allroggen, N., van Schaik, L., Wienhöfer, J., and  
816 Zehe, E.: Picturing and modeling catchments by representative hillslopes, *Hydrol. Earth  
817 Syst. Sci.*, 21, 1225-1249, 10.5194/hess-21-1225-2017, 2017.
- 818 Loritz, R., Gupta, H., Jackisch, C., Westhoff, M., Kleidon, A., Ehret, U., and Zehe, E.: On the  
819 dynamic nature of hydrological similarity, *Hydrol. Earth Syst. Sci. Discuss.*,  
820 <https://doi.org/10.5194/hess-2017-739>, in review, 2018.
- 821 Lotka, A. J.: Contribution to the energetics of evolution, *Proc Natl Acad Sci USA*, 8, 147-151,  
822 1922a.

- 823 Lotka, A. J.: Natural selection as a physical principle, *Proc Natl Acad Sci USA*, 8, 151-154,  
824 1922b.
- 825 Martinez-Carreras, N., Wetzel, C. E., Frentress, J., Ector, L., McDonnell, J. J., Hoffmann, L.,  
826 and Pfister, L.: Hydrological connectivity inferred from diatom transport through the  
827 riparian-stream system, *Hydrology And Earth System Sciences*, 19, 3133-3151,  
828 10.5194/hess-19-3133-2015, 2015.
- 829 Nobre, A. D., Cuartas, L. A., Hodnett, M., Renno, C. D., Rodrigues, G., Silveira, A.,  
830 Waterloo, M., and Saleska, S.: Height above the nearest drainage - a hydrologically  
831 relevant new terrain model, *Journal Of Hydrology*, 404, 13-29,  
832 10.1016/j.jhydrol.2011.03.051, 2011.
- 833 Paltridge, G. W.: Climate and thermodynamic systems of maximum dissipation, *Nature*, 279,  
834 630-631, 10.1038/279630a0, 1979.
- 835 Pfister, L., Iffly, J., and Hoffmann, L.: Use of regionalized stormflow coefficients with a view  
836 to hydroclimatological hazard mapping, *Hydrological Sciences Journal-Journal Des*  
837 *Sciences Hydrologiques*, 47, 479-491, 2002.
- 838 Pfister, L., Martinez-Carreras, N., Hissler, C., Klaus, J., Carrer, G. E., Stewart, M. K., and  
839 McDonnell, J. J.: Bedrock geology controls on catchment storage, mixing, and release:  
840 A comparative analysis of 16 nested catchments, *Hydrological Processes*, 31, 1828-  
841 1845, 10.1002/hyp.11134, 2017.
- 842 Porada, P., Kleidon, A., and Schymanski, S. J.: Entropy production of soil hydrological  
843 processes and its maximisation, *Earth Syst. Dynam.*, 2, 179-190, 10.5194/esd-2-179-  
844 2011, 2011.
- 845 Reggiani, P., Hassanizadeh, S. M., and Sivapalan, M.: A unifying framework for watershed  
846 thermodynamics: Balance equations for mass, momentum, energy and entropy, and the  
847 second law of thermodynamics, *Advances in Water Resources*, 22, 367-398, 1998a.
- 848 Reggiani, P., Sivapalan, M., and Hassanizadeh, S. M.: A unifying framework for watershed  
849 thermodynamics: Balance equations for mass, momentum, energy and entropy, and the  
850 second law of thermodynamics, *Advances In Water Resources*, 22, 367-398, 1998b.
- 851 Reggiani, P., Hassanizadeh, S. M., Sivapalan, M., and Gray, W. G.: A unifying framework for  
852 watershed thermodynamics: Constitutive relationships, *Advances In Water Resources*,  
853 23, 15-39, 1999.
- 854 Reggiani, P., Sivapalan, M., and Hassanizadeh, S. M.: Conservation equations governing  
855 hillslope responses: Exploring the physical basis of water balance, *Water Resources*  
856 *Research*, 36, 1845-1863, 2000.
- 857 Reggiani, P., and Schellekens, J.: Modelling of hydrological responses: The representative  
858 elementary watershed approach as an alternative blueprint for watershed modelling,  
859 *Hydrological Processes*, 17, 3785-3789, 2003.
- 860 Renner, M., Hassler, S. K., Blume, T., Weiler, M., Hildebrandt, A., Guderle, M., Schymanski,  
861 S. J., and Kleidon, A.: Dominant controls of transpiration along a hillslope transect  
862 inferred from ecohydrological measurements and thermodynamic limits, *Hydrology*  
863 *And Earth System Sciences*, 20, 2063-2083, 10.5194/hess-20-2063-2016, 2016.
- 864 Renno, C. D., Nobre, A. D., Cuartas, L. A., Soares, J. V., Hodnett, M. G., Tomasella, J., and  
865 Waterloo, M. J.: Hand, a new terrain descriptor using srtm-dem: Mapping terra-firme

- 866 rainforest environments in amazonia, *Remote Sensing of Environment*, 112, 3469-3481,  
867 10.1016/j.rse.2008.03.018, 2008.
- 868 Rinaldo, A., Maritan, A., Colaiori, F., Flammini, A., and Rigon, R.: Thermodynamics of  
869 fractal networks, *Physical Review Letters*, 76, 3364-3367, 1996.
- 870 Saco, P. M., and Moreno-de las Heras, M.: Ecogeomorphic coevolution of semiarid  
871 hillslopes: Emergence of banded and striped vegetation patterns through interaction of  
872 biotic and abiotic processes, *Water Resources Research*, 49, 115-126,  
873 10.1029/2012wr012001, 2013.
- 874 Savenije, H. H. G., and Hrachowitz, M.: Hess opinions "catchments as meta-organisms - a  
875 new blueprint for hydrological modelling", *Hydrology And Earth System Sciences*, 21,  
876 1107-1116, 10.5194/hess-21-1107-2017, 2017.
- 877 Schneider, A. K., Hohenbrink, T. L., Reck, A., Zangerle, A., Schroder, B., Zehe, E., and van  
878 Schaik, L.: Variability of earthworm-induced biopores and their hydrological  
879 effectiveness in space and time, *Pedobiologia*, 71, 8-19, 10.1016/j.pedobi.2018.09.001,  
880 2018.
- 881 Seibert, S. P., Jackisch, C., Ehret, U., Pfister, L., and Zehe, E.: Unravelling abiotic and biotic  
882 controls on the seasonal water balance using data-driven dimensionless diagnostics,  
883 *Hydrology And Earth System Sciences*, 21, 2817-2841, 10.5194/hess-21-2817-2017,  
884 2017.
- 885 Sivapalan, M., and Blöschl, G.: Time scale interactions and the coevolution of humans and  
886 water, *Water Resources Research*, 51, 6988-7022, 10.1002/2015wr017896, 2015.
- 887 Sivapalan, M.: From engineering hydrology to earth system science: Milestones in the  
888 transformation of hydrologic science, *Hydrology And Earth System Sciences*, 22, 1665-  
889 1693, 10.5194/hess-22-1665-2018, 2018.
- 890 Tian, F., Hu, H., Lei, Z., and Sivapalan, M.: Extension of the representative elementary  
891 watershed approach for cold regions via explicit treatment of energy related processes,  
892 *Hydrology And Earth System Sciences*, 10, 619-644, 2006.
- 893 Tietjen, B., Zehe, E., and Jeltsch, F.: Simulating plant water availability in dry lands under  
894 climate change: A generic model of two soil layers, *Water Resources Research*, 45,  
895 W01418 10.1029/2007wr006589, 2009.
- 896 Troch, P. A., Lahmers, T., Meira, A., Mukherjee, R., Pedersen, J. W., Roy, T., and Valdes-  
897 Pineda, R.: Catchment coevolution: A useful framework for improving predictions of  
898 hydrological change?, *Water Resources Research*, 51, 4903-4922,  
899 10.1002/2015wr017032, 2015.
- 900 Westhoff, M. C., and Zehe, E.: Maximum entropy production: Can it be used to constrain  
901 conceptual hydrological models?, *Hydrology And Earth System Sciences*, 17, 3141-  
902 3157, 10.5194/hess-17-3141-2013, 2013.
- 903 Westhoff, M. C., Zehe, E., and Schymanski, S. J.: Importance of temporal variability for  
904 hydrological predictions based on the maximum entropy production principle,  
905 *Geophysical Research Letters*, 41, 67-73, 10.1002/2013gl058533, 2014.
- 906 Westhoff et
- 907 Zehe, E., Lee, H., and Sivapalan, M.: Dynamical process upscaling for deriving catchment  
908 scale state variables and constitutive relations for meso-scale process models,  
909 *Hydrology And Earth System Sciences*, 10, 981-996, 2006.

- 910 Zehe, E., Blume, T., and Bloschl, G.: The principle of 'maximum energy dissipation': A novel  
911 thermodynamic perspective on rapid water flow in connected soil structures, *Philos.*  
912 *Trans. R. Soc. B-Biol. Sci.*, 365, 1377-1386, 10.1098/rstb.2009.0308, 2010.
- 913 Zehe, E., Graeff, T., Morgner, M., Bauer, A., and Bronstert, A.: Plot and field scale soil  
914 moisture dynamics and subsurface wetness control on runoff generation in a headwater  
915 in the ore mountains, *Hydrol. Earth Syst. Sci. Discuss*, 14, 873–889, doi:10.5194/hess-  
916 14-873-2010, 2010.
- 917 Zehe, E., Ehret, U., Blume, T., Kleidon, A., Scherer, U., and Westhoff, M.: A thermodynamic  
918 approach to link self-organization, preferential flow and rainfall-runoff behaviour,  
919 *Hydrology And Earth System Sciences*, 17, 4297-4322, 10.5194/hess-17-4297-2013,  
920 2013.
- 921 Zehe, E., Ehret, U., Pfister, L., Blume, T., Schroder, B., Westhoff, M., Jackisch, C.,  
922 Schymanski, S. J., Weiler, M., Schulz, K., Allroggen, N., Tronicke, J., van Schaik, L.,  
923 Dietrich, P., Scherer, U., Eccard, J., Wulfmeyer, V., and Kleidon, A.: Hess opinions:  
924 From response units to functional units: A thermodynamic reinterpretation of the hru  
925 concept to link spatial organization and functioning of intermediate scale catchments,  
926 *Hydrology And Earth System Sciences*, 18, 4635-4655, 10.5194/hess-18-4635-2014,  
927 2014.
- 928 Zhang, L., Savenije, H. H. G., Fenicia, F., and Pfister, L.: Modelling subsurface stream flow  
929 with the representative elementary watershed (rew) approach: Application to the alzette  
930 river basin, *HESSD-2005-0118*, 2006.
- 931 Zhang, Z. L., and Savenije, H. H. G.: Thermodynamics of saline and fresh water mixing in  
932 estuaries, *Earth System Dynamics*, 9, 241-247, 10.5194/esd-9-241-2018, 2018.  
933